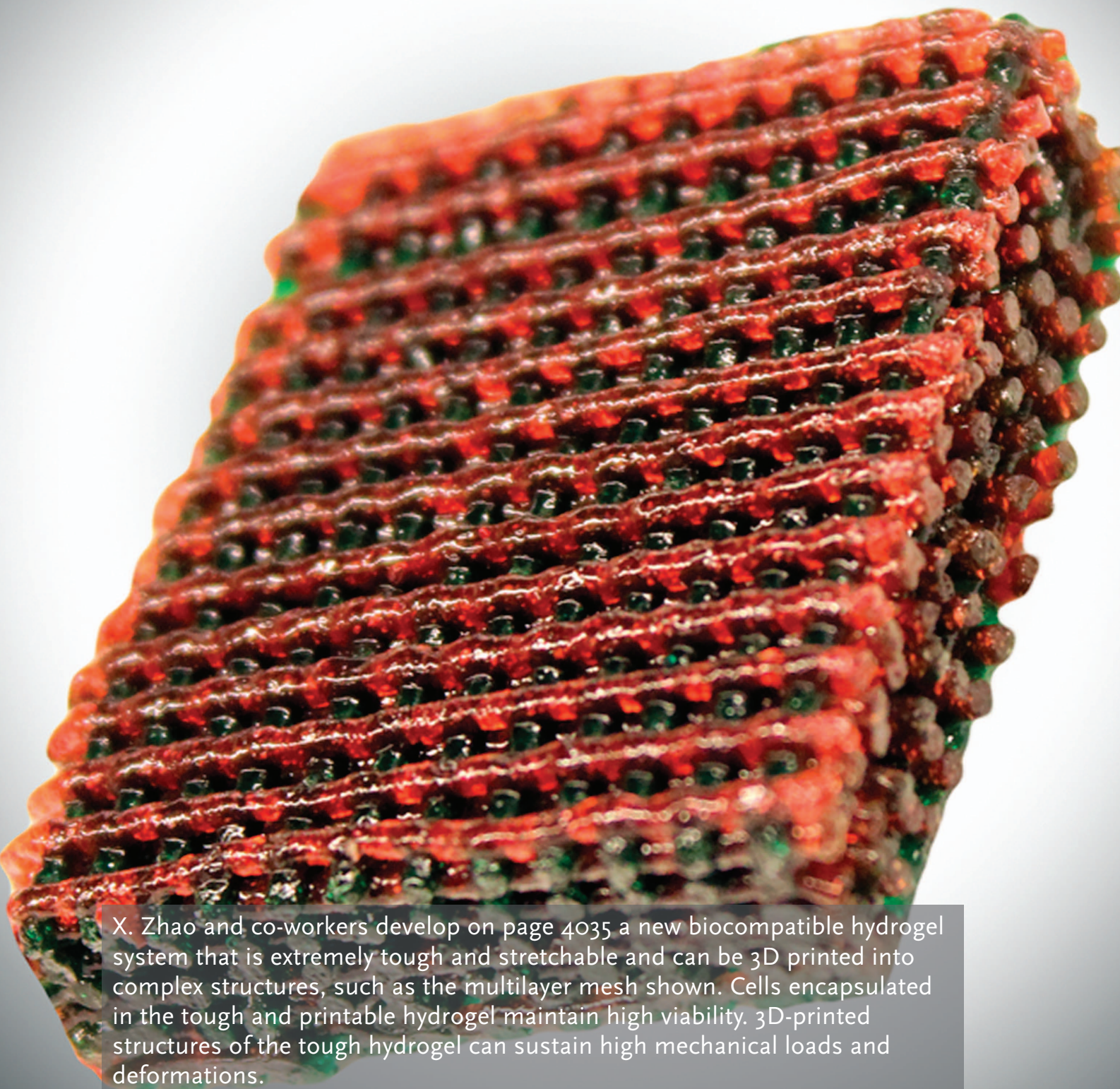# ADVANCED MATERIALS

X. Zhao and co-workers develop on page 4035 a new biocompatible hydrogel system that is extremely tough and stretchable and can be 3D printed into complex structures, such as the multilayer mesh shown. Cells encapsulated in the tough and printable hydrogel maintain high viability. 3D-printed structures of the tough hydrogel can sustain high mechanical loads and deformations.

3D PRINTING

3D Printing of Highly Stretchable and Tough Hydrogels into Complex, Cellularized Structures

*Sungmin Hong, Dalton Sycks, Hon Fai Chan, Shaoting Lin, Gabriel P. Lopez, Farshid Guilak, Kam W. Leong, and Xuanhe Zhao**

Living tissues usually have high fracture toughness in order to withstand substantial internal and external mechanical loads.[1] The high toughness of tissues challenges researchers to design hydrogels capable of achieving similar toughness in order to withstand physiological mechanical loads.[2] Despite recent success in developing tough hydrogels,[3–12] the fabrication of these hydrogels often involves toxic chemicals and/or harsh reactions, limiting their capability to encapsulate cells. In addition, it is desirable to fabricate cell-embedded hydrogels with macroporous architecture conducive to generation of complex tissues. While 3D printing offers rapid prototyping[13–17] and can print hydrogels into complex 3D structures for functions such as vascular networks[14,16] and aortic valves,[18,19] it has not been possible to print tough hydrogels into complex structures other than simple and flat ones such as dog-bone samples.[15]

Here, we chose the biocompatible materials sodium alginate and poly (ethylene glycol) (PEG) to constitute an interpenetrating network (**Figure 1**). The resultant hydrogel of covalently crosslinked PEG and ionically crosslinked alginate possesses high fracture toughness and allows cell encapsulation (**Figures 2** and **3**). (Detailed formulation of the hydrogel is

Dr. S. Hong, D. Sycks, S. Lin, Prof. G. P. Lopez,
Prof. F. Guilak, Prof. X. Zhao
Department of Mechanical Engineering
and Material Science
Duke University
Durham, NC 27708, USA
E-mail: zhaox@mit.edu
H. F. Chan, Prof. G. P. Lopez, Prof. F. Guilak, Prof. K. W. Leong
Department of Biomedical Engineering
Duke University
Durham, NC 27708, USA
S. Lin, Prof. X. Zhao
Department of Mechanical Engineering
Massachusetts Institute of Technology
Cambridge, MA 02139, USA
Prof. F. Guilak
Department of Orthopaedic Surgery
Duke University Medical Center
Durham, NC 27710, USA
Prof. K. W. Leong
Department of Biomedical Engineering
Columbia University
New York, NY 10027, USA
Prof. X. Zhao
Department of Civil and Environmental Engineering
Massachusetts Institute of Technology
Cambridge, MA 02139, USA

described in the Experimental Section.) We hypothesize that the toughening of this biocompatible hydrogel relies on a combination of two mechanisms: the reversible Ca^{2+} crosslinking of alginate dissipates mechanical energy, while the covalent crosslinking of PEG maintains elasticity under large deformations (Figure 1). To test this hypothesis, we varied the molecular weight of PEG (6000–20 000 Da) and the concentrations of Ca^{2+} (25 µL of either 0 or 1 M $CaSO_4$ solution added per 1 mL of the pre-gel PEG–alginate mixture) in the hydrogels, and used pure-shear tests to measure the fracture energies of the resultant hydrogels.[20] (Details of the pure-shear test are described in Figure S1, Supporting Information.) As shown in Figure S2a (Supporting Information), the fracture energies of hydrogels without Ca^{2+} are consistently low (below 211 J m^{-2}) and they display negligible stress–strain hysteresis (Figure S2b, Supporting Information). Introducing reversible Ca^{2+} crosslinking into the hydrogels significantly increases their fracture energies. The increase in fracture energy is also accompanied by significant increase in stress–strain hysteresis, which indicates mechanical dissipation in the hydrogels under deformation (Figure S2b, Supporting Information). In addition, the fracture energy of calcium-containing hydrogels increases drastically with the molecular weight of PEG, because the longer polymer chains of PEG allow for higher stretchability of the hydrogel (Figure S2a,c, Supporting Information). These results validate the hypothesis that the combined mechanisms of mechanical energy dissipation and high elasticity are critical to the toughening of the PEG–alginate hydrogels. To further test the hypothesis, we made a set of pure PEG hydrogels with different molecular weights and concentrations of PEG and measured their fracture energies. From Figures S2a and S3 (Supporting Information), it is evident that the fracture energies of pure PEG hydrogels are significantly lower than the corresponding PEG–alginate hydrogels with Ca^{2+}, further validating the proposed toughening mechanism.

By further optimizing the concentrations of polymers and photoinitiators (Figures S3 and S4, Supporting Information), the resultant hydrogel with 20 wt% PEG and 2.5 wt% alginate can reach a maximum fracture energy of ≈1500 J m^{-2}, which is higher than the value of articular cartilage.[21] Furthermore, we used a digital image correlation technique[22] to measure the stress field around the tip of a crack in the hydrogel under pure shear tests. (Details of the digital image correlation technique are described in the Experimental Section and in Figure S5, Supporting Information.) As shown in Figure 2a, the crack in the hydrogel becomes highly blunted and the principal stress/strain at the crack tip before crack propagation reaches approximately the ultimate tensile strength/strain of the same,
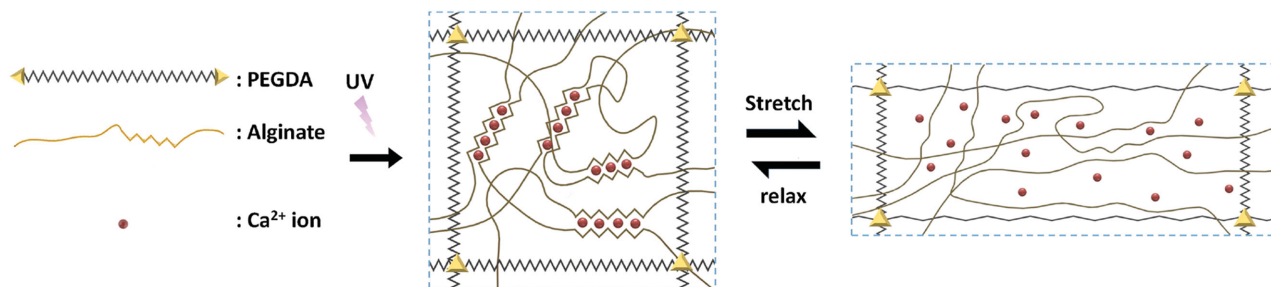
COMMUNICATION

Figure 1. Schematic diagrams of the biocompatible and tough hydrogel. PEG and alginate polymers are covalently and ionically crosslinked through UV exposure and Ca^{2+}, respectively. As the hydrogel is deformed, the alginate chains are detached from the reversible ionic crosslinks and mechanical energy is dissipated. Once the hydrogel is relaxed from deformation, it regains its original configuration since the covalently crosslinked PEG network maintains the elasticity of the hydrogel. Over time, some of the ionic crosslinks in the alginate network can reform in the deformed and relaxed hydrogel.

unnotched hydrogel under pure-shear tension (Figure 2b). The result indicates that the alginate–PEG hydrogel behaves as a tough, soft material during fracture.[23]

In addition, since the mechanical energy dissipation in the PEG–alginate hydrogel relies on reversible crosslinking, the dissipative property of the hydrogel is partially recoverable after deformation.[3] We illustrated this point by stretching a hydrogel sample with the optimized composition to a strain of 400%, followed by relaxation of the sample. The relaxed sample was then kept in a humid chamber at 37 °C, and we repeated the stretch–relax tests after 30 min and 24 h of storage. Figure 2c shows that after storage at 37 °C for 24 h, the deformed hydrogel can achieve 58.9% of the hysteresis in the first loading–unloading

cycle, indicating partial recovery of the dissipative properties due to reversible crosslinking of Ca^{2+}.

The recovery of ionic crosslinking responsible for energy dissipation contributes to the maintenance of relatively high fracture energy of the hydrogel after deformation.[24,3] To demonstrate this point, we stretched a set of hydrogels to different strains, ranging from 0% to 500%, under uniaxial tension. The fracture energies of the predeformed hydrogels were measured either right after the prestrain or after storage in a humid chamber at 37 °C for 24 h. The measured fracture energies of hydrogels under different prestrains are given in Figure 2d. It can be seen that prestrained hydrogels have drastically reduced fracture energies if tested immediately after deformation, since the dissipative ionic crosslinks do not have enough time to reform. On the other hand, if prestrained hydrogels are stored at 37 °C for 24 h, they can recover most of their fracture energy. For example, a hydrogel subjected to a large strain of 500% and then stored at 37 °C for 24 h recovered 70.5% of the fracture energy of the undeformed gel. Such retention of fracture toughness after deformation is critical to the design of antifatigue hydrogels.[4,6]

Both PEG and alginate are widely known to be biocompatible and have been extensively used in biomedical applications.[25,26] We hypothesize that the tough PEG–alginate hydrogel can be used to encapsulate cells while maintaining high viability of the encapsulated cells for biomedical applications. To test this hypothesis, human mesenchymal stem cells (hMSCs) encapsulated in the hydrogels were monitored for viability. Before encapsulation, 2 mL of PEG–alginate mixture was prepared, and the hMSC suspension was centrifuged at 1000 rpm for 5 min. The cell pellet was resuspended with 70 µL of I-2959 (1%, w/vol in H_2O) and mixed with poly (ethylene glycol) diacrylate (PEGDA)–alginate solution to seed a final cell density of 3×10^6 cells mL^{-1}. Then, 50 µL of $CaSO_4 \cdot 2H_2O$ slurry was thoroughly mixed into the hydrogel, which was then
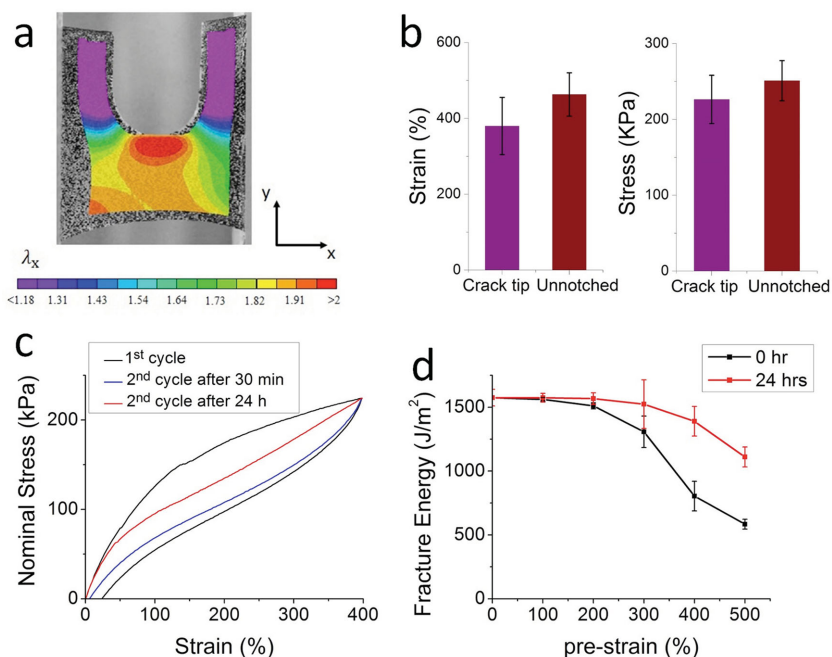

Figure 2. Mechanical properties of the hydrogel. a) Stretch along x-direction in a notched sample of the hydrogel under pure-shear test. b) Comparison of the critical strain and stress at the crack tip before crack propagation and the failure strain and stress of a sample without notch under pure-shear tension. c) Stress–strain hysteresis of the hydrogel under the first and second cycles of deformation. The sample was stored in a humid chamber at 37 °C for 5 min or 24 h between the two cycles of deformation. d) Fracture energies of hydrogels predeformed to different strains. The fracture energies were measured right after the predeformation or after storing the hydrogel in a humid chamber at 37 °C for 24 h.
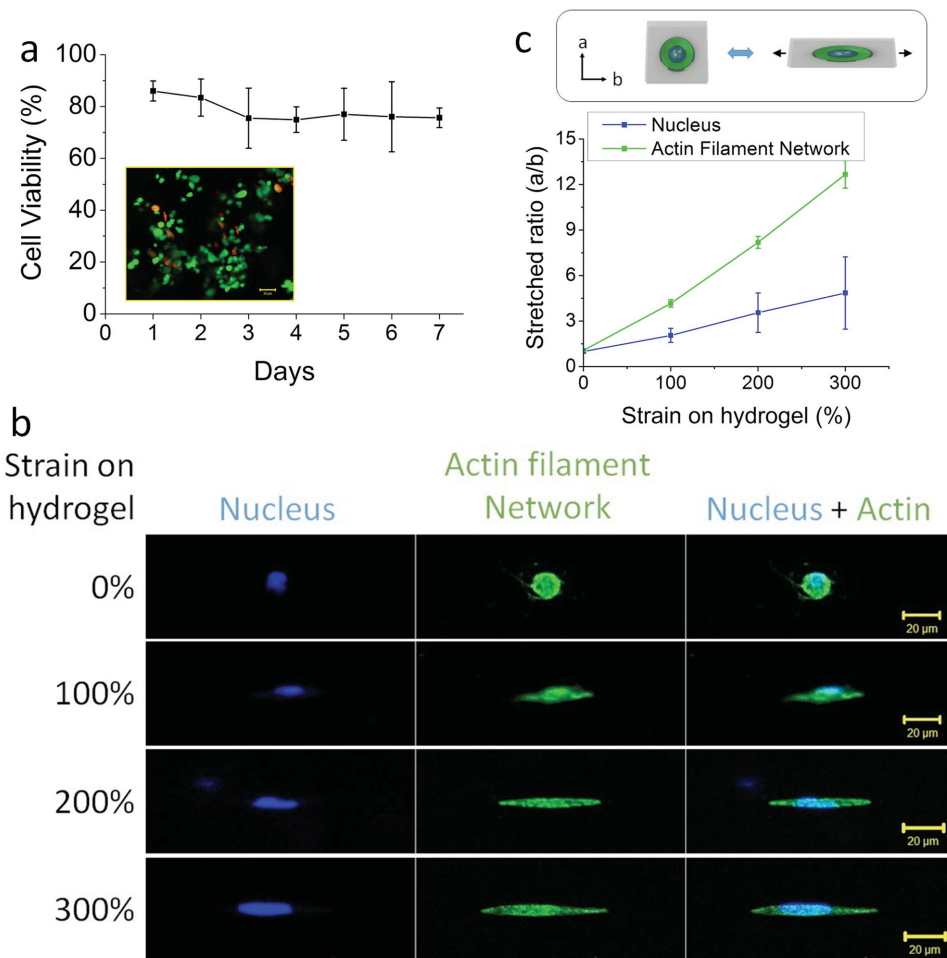
Materials
Views

www.MaterialsViews.com

ADVANCED
MATERIALS
www.advmat.de

COMMUNICATION

Figure 3. hMSC encapsulation in the hydrogel. a) hMSC viability results over 7 d (inset: Live/dead assay images after 7 d from encapsulation). b) Deformation of the hMSC encapsulated in the hydrogel matrix, which was stretched to different strains. c) Ratio of nucleus and cell body as a function of the applied strain on the hydrogel matrix.

transferred to a glass mold and exposed to 365 nm UV light for 10 min to crosslink the solution into PEG–alginate hydrogel. The hydrogel was immersed in α-minimum essential medium with 20% fetal bovine serum and 1% penicillin/streptomycin. Live/dead assays were used to determine cell viability in the hydrogel over the course of 7 d. From Figure 3a, it can be seen that high cell viability, ranging from 86.0 ± 3.8% to 75.5 ± 11.6%, was maintained over 7 d of culture. The result indicates that the current synthesis of the PEG–alginate hydrogel is a benign, cell-friendly process and the resultant hydrogel allows for nutrient diffusion and waste transport to support viable cell culture over extended periods of time.

Because the PEG–alginate hydrogel is highly stretchable and tough, the hMSCs encapsulated in this 3D extracellular matrix can be highly deformed by stretching the hydrogel. To illustrate this point, the hydrogel with encapsulated hMSCs was stretched to various strains from 0% to 300%, and then fixed on a glass slide. The stretched gels were imaged under a Zeiss LSM 510 inverted confocal laser microscope. As shown in Figure 3b, both the actin-filament network and nuclei were highly deformed together with the gel.

Consequently, the ratio between two axes of cell bodies and nuclei drastically increased with applied strains, as shown in Figure 3c.

Next, we demonstrate the capability of printing the PEG–alginate hydrogels into various complicated 3D structures that can also be cellularized. Controlling the viscosity of the pregel solution is critical to the success of printing 3D structures of hydrogels.[14,15,27] It is usually desirable for the pre-gel solution to have relatively low viscosity at high shear rate but much higher viscosity at low shear rate, so that the pre-gel solution can easily flow out of the printer but maintain its shape once printed.[18,19,28] Here, we chose to use biocompatible nanoclay (Laponite XLG, BYK Additives, Inc., TX, USA) to control the viscosity of the pre-gel solution[29] by incorporating it into the PEG–alginate hydrogel. The nanoclay particles physically crosslink both with themselves, as well as with the polymer networks of the PEG and alginate to increase the viscosity of the pre-gel solution.[30,31] A cone and plate rheometer (TA Instruments, New Castle, DE, USA) was used to confirm the increase in viscosity of the pre-gel solution as a function of nanoclay content, while maintaining its ability to shear thin and flow under the
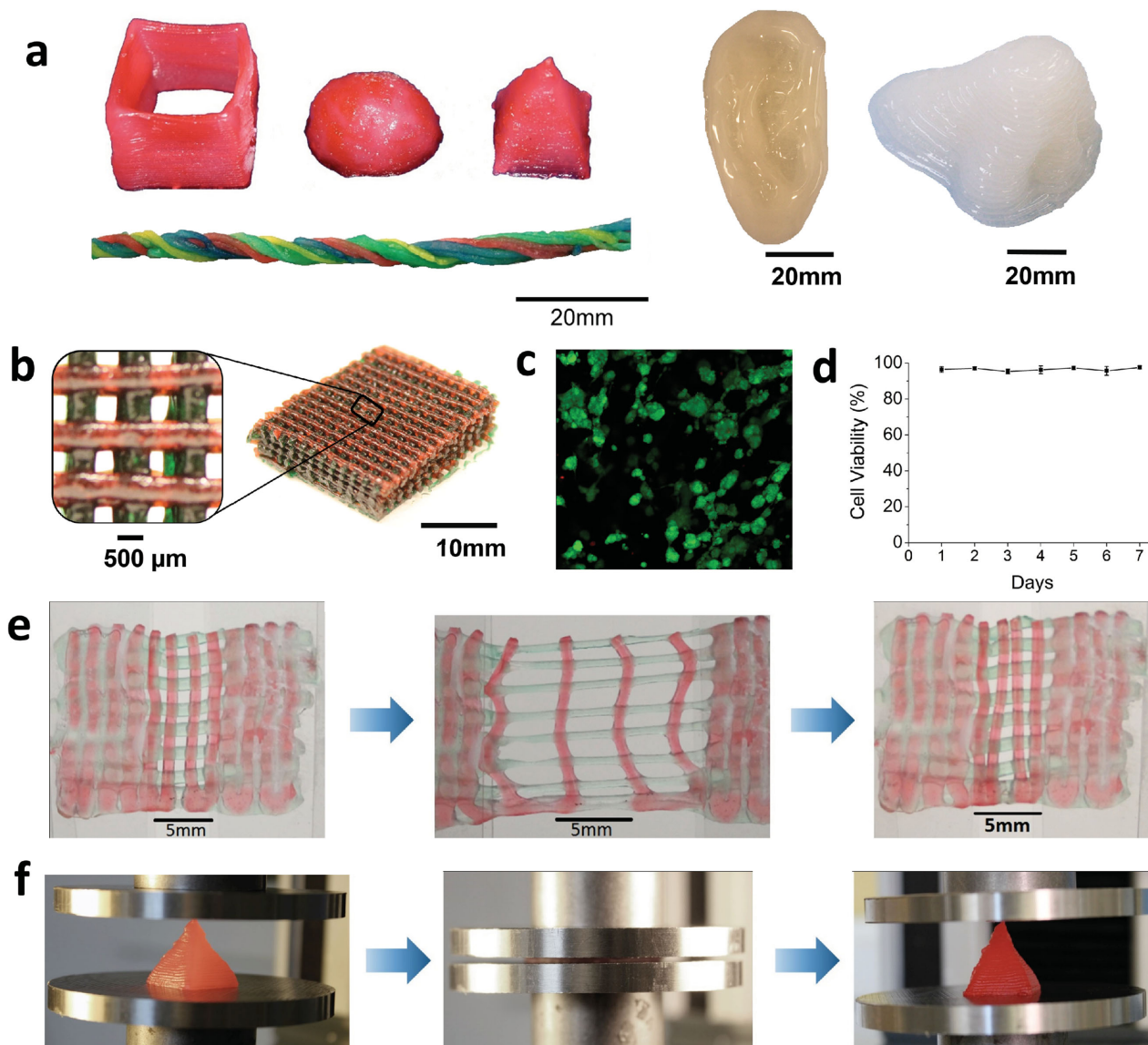
Figure 4. 3D printing of tough and biocompatible PEG–alginate–nanoclay hydrogels. a) Various 3D constructs printed with the hydrogel (from left to right: hollow cube, hemisphere, pyramid, twisted bundle, the shape of an ear, and a nose. Nontoxic red food dye was added postprint on some samples for visibility). b) A mesh printed with the tough and biocompatible hydrogel. The mesh was used to host HEK cells. c) Live-dead assay of HEK cells in a collagen hydrogel infused into the 3D printed mesh of the PEG–alginate–nanoclay hydrogel. d) Viability of the HEK cells through 7 d. e) A printed bilayer mesh (top layer red, bottom layer green) is uniaxially stretched to three times of its initial length. Relaxation of the sample after stretching shows almost complete recovery of its original shape. f) A printed pyramid undergoes a compressive strain of 95% while returning to its original shape after relaxation.

high shear rates present in the extrusion needle (Figure S6, Supporting Information).

Because nanoclay significantly enhances the viscosity of the pre-gel solution and also increases its shear-thinning properties, we chose the PEG–alginate–nanoclay system as the ink of our 3D printer (Fab@Home Model 3, Seraph Robotics, Inc., NY, USA). The printing process is described in the Experimental Section. In **Figure 4**a and Movie 1 (Supporting Information), we show that the PEG–alginate–nanoclay hydrogels can be printed into diverse shapes such as a hollow cube, hemisphere, pyramid, twisted bundle, and physiologically relevant shapes such as human nose and ear models. Printed objects

may also be composed of multiple materials, which is illustrated in the two-color mesh in Figure 4b. The mesh consists of alternating layers of PEG–alginate–nanoclay that either contains red or green food dye to demonstrate this concept. The spatial resolution of the printed objects depends on factors such as precision of the printer, the pre-gel viscosity, and extrusion needle diameter, and is ≈500 μm with the current printer. This resolution is consistent with previous reports on hydrogel structures printed with the same type of printer (i.e., Fab@Home).[18,19] Tough hydrogel structures of higher resolution may be achieved by using the PEG–alginate–nanoclay system with a 3D printer of higher precision.

To investigate the biocompatibility of the printed tough hydrogel with incorporated nanoclay, human embryonic kidney (HEK) cells were encapsulated into a type 1 rat tail collagen solution (Corning Inc., Corning, NY, USA), which then gelled throughout the interconnected pores of the printed PEG–alginate–nanoclay mesh to form a composite hydrogel (Figure S7, Supporting Information). The encapsulated HEK cells were seeded at a concentration of 3×10^6 cells mL^{-1} of collagen gel, and maintained high viability ($\approx$95%) over the course of 7 d of culture (Figure 4c,d).

The printed hydrogel structures are also highly deformable and tough, demonstrating that the added nanoclay does not significantly affect the superior mechanical qualities of the hydrogel. As shown in Figure 4e, a printed mesh of the hydrogel was uniaxially stretched to 300% of its undeformed length, held for 1 min, and allowed to relax to its initial state. The mesh experienced very little permanent deformation, since the long-chain PEG network maintains the high elasticity of the hydrogel. Figure 4f and Movie 2 (Supporting Information) show a printed pyramid that undergoes 95% compressive strain and regains 97% of its original height within 5 min of unloading.

In conclusion, we have created a tough hydrogel comprised of PEG and sodium alginate that can be used for cell encapsulation. The hydrogel can endure high stress in both tension and compression and has a fracture toughness above 1500 J m^{-2}, making it tougher than natural cartilage and yet with water content ($\approx$77.5 wt%) that is tunable and within the physiologically acceptable range. The reversible crosslinking of the alginate dissipates mechanical energy under deformation and the long-chain PEG network maintains high elasticity of the hydrogel; these phenomena combine to result in a robust, tough hydrogel. Encapsulated cells showed high viability over 7 d, averaging 75.5 ± 11.6% in the PEG–alginate hydrogel and 95% in infiltrated collagen between the pores of a printed PEG–alginate–nanoclay mesh. In addition, we were able to print the tough hydrogel into complicated 3D structures by using nanoclay to control the pre-gel solution's viscosity. To our knowledge, this study is the first to demonstrate a hydrogel that is not only tough and 3D-printable, but suitable for long-term cell culture as well.

Experimental Section

PEG–Alginate Hydrogel Fabrication: PEG powder was purchased from Sigma Aldrich and modified into PEGDA according to previously published protocols[32] and dissolved in deionized (DI) water (40 wt%). Brown sodium alginate solution in water (5 wt%) was mixed with the 40% PEGDA solution. After degassing the solution in a vacuum chamber, Irgacure 2959 (I-2959) and calcium sulfate slurry (1 M CaSO$_4$·2H$_2$O) were added as photoinitiator for PEGDA and ionic crosslinker for alginate, respectively. The mixture was then carefully poured into a glass mold and cured under ultraviolet light (365 nm wavelength) for 10 min. PEGDA chains covalently crosslink via radicals generated from the photoinitiator (I-2959) when exposed to UV and form a covalent, ductile network capable of large deformation. In contrast, alginate is ionically crosslinked in the presence of divalent cations (such as Ca^{2+}) and imparts stiffness into the network. After curing, mechanical tests were performed at room temperature using a dynamic mechanical analyzer (RSA III, TA instruments, DE, USA).

Digital Image Correlation: As is illustrated by Figure S5 (Supporting Information), digital image correlation is a noncontact optical technique that allows full-field strain measurement on a surface under deformation.[33] A random speckle pattern was generated on the surface of a sample via spray painting. Images of speckle patterns at both the reference state and deformed state were recorded by a standard video camera during the process of the deformation. Based on the video, the commercial software VIC-2D (Correlated Solutions Inc., Columbia, SC, USA) was applied to measure strain mapping of the deformed sample. Essentially, both images were transformed to grayscale matrices. To track the surface displacements of deforming materials, a mathematically well-defined correlated function was applied to match digitalized images before deformation and after deformation

$$r(x,y) = 1 - \frac{\sum A(x,y)B(x^*,y^*)}{\left(\sum A(x,y)^2 \times \sum B(x^*,y^*)^2\right)^{1/2}} \quad (1)$$

$A(x, y)$ is the gray level at the location of (x, y) at reference state, $B(x^*, y^*)$ represents the gray level at the location of (x^*, y^*) at deformed state. The relation between (x^*, y^*) and $A(x, y)$ can be related as

$$\begin{cases} x^* = x + u + \dfrac{\partial u}{\partial x}\Delta x + \dfrac{\partial u}{\partial y}\Delta y \\[2mm] y^* = y + v + \dfrac{\partial v}{\partial x}\Delta x + \dfrac{\partial v}{\partial y}\Delta y \end{cases} \quad (2)$$

where u and v respectively represent the displacements in the direction of x and y. The displacements can be determined by minimizing the correlation function $r(x, y)$.

Cell Culture: Bone marrow–derived hMSCs were provided by Tulane University Health Sciences Centre and cultured in α-minimum essential medium supplemented with 20% fetal bovine serum and 1% penicillin/streptomycin at 37 °C and 5% CO$_2$. The 4–7th passages of hMSCs were used in this study. Human Embryonic Kidney 293 cell (HEK-293) line was obtained from ATCC (Manassas, VA, USA) and cultured in Dulbecco's modified eagle medium (high glucose) with 10% fetal bovine serum and 1% penicillin/streptomycin. Cells were trypsinized with 0.25% trypsin–ethylenediaminetetraacetic acid (EDTA, Life Technologies, Grand Island, NY, USA) before being counted and mixed with the gel precursor solution.

Viability Test: To perform viability testing, the samples were washed in 1× Dulbecco's phosphate buffered saline before soaking in 2×10^{-6} M Calcein AM (Sigma-Aldrich, St. Louis, MO, USA) and 5×10^{-6} M propidium iodide (Sigma-Aldrich, St. Louis, MO, USA) solution for 30 min. Fluorescent images were taken using Zeiss LSM 510 inverted confocal microscope provided by Duke University Light Microscopy Core Facility.

Collagen Gel Preparation for Cell Encapsulation: Type 1 rat tail collagen (Corning Inc., Corning, NY, USA) was diluted with 0.6% acetic acid (Sigma-Aldrich, St. Louis, MO, USA) to a final collagen concentration of 2 mg mL^{-1}. This solution was neutralized with 5 M NaOH (Sigma-Aldrich, St. Louis, MO, USA), and 10× α-minimum essential media (Sigma-Aldrich, St. Louis, MO, USA) was added to a final concentration of 1×. HEK cells were added, and the solution formed a gel over the course of 30 min of incubation at room temperature.

Cell Staining for Stretch Testing: The samples were fixed with 4% paraformaldehyde (Electron Microscopy Sciences, Hatfield, PA, USA) for 30 min before staining with Alexa Fluor 488 Phalloidin for the actin-filament network (Life Technologies, Grand Island, NY, USA) and DAPI for the nucleus (Sigma-Aldrich, St. Louis, MO, USA) for 1 h. The samples were washed with PBS for three times before being mounted on a glass slide for imaging.

3D Printing PEG–Alginate–Nanoclay Hydrogel: PEGDA–alginate mixture was prepared as described above, but Laponite XLG (final concentration 5 wt%) was first dissolved into deionized water, followed by PEGDA. This gel was allowed to homogenize and settle overnight, after which it was mixed in a 1:1 ratio with the 5 wt% alginate solution and allowed to equilibrate for one additional day. After degassing,

I-2959 and CaSO$_4$ solution were added to the pre-gel solution. The PEGDA–alginate–nanoclay pre-gel solution was then loaded into extrusion cartridges, which were placed on the printing carriage of 3D printer for extrusion through a 15G-20G flat tip needle. During printing, the pre-gel solution experienced shear thinning inside the extrusion needle, and quickly regained its viscosity upon exiting. Following extrusion, all flat, printed shapes were encased in glass slides and placed in the UV chamber to complete covalent crosslinking of the PEGDA polymer chains. 3D shapes were crosslinked in a sealed, nitrogenous environment under a 100 mW cm^{-2} UV source with emission peaks centered on 365 nm. Since the viscosity of hydrogel was enhanced by adding nanoclay, it was able to be printed into various shapes free from vertical limitation (Figure 4a). Controlling the concentration of nanoclay in the gel permits the viscosity to be optimized for extrusion-based printing while still maintaining 3D structures without requiring support material (Figure S4, Supporting Information).

Supporting Information

Supporting Information is available from the Wiley Online Library or from the author.

Acknowledgements

[1] D. Taylor, N. O'Mara, E. Ryan, M. Takaza, C. Simms, *J. Mech. Behav. Biomed. Mater.* **2012**, *6*, 139.

[2] B. O. Diekman, N. Christoforou, V. P. Willard, H. Sun, J. Sanchez-Adams, K. W. Leong, F. Guilak, *Proc. Natl. Acad. Sci. U. S. A.* **2012**, *109*, 19172.

[3] J.-Y. Sun, X. Zhao, W. R. K. Illeperuma, O. Chaudhuri, K. H. Oh, D. J. Mooney, J. J. Vlassak, Z. Suo, *Nature* **2012**, *489*, 133.

[4] T. L. Sun, T. Kurokawa, S. Kuroda, A. B. Ihsan, T. Akasaki, K. Sato, M. A. Haque, T. Nakajima, J. P. Gong, *Nat. Mater.* **2013**, *12*, 932.

[5] C. M. Hassan, N. A. Peppas, *Macromolecules* **2000**, *33*, 2472.

[6] X. Zhao, *Soft Matter* **2014**, *10*, 672.

[7] I. C. Liao, F. T. Moutos, B. T. Estes, X. Zhao, F. Guilak, *Adv. Funct. Mater.* **2013**, *23*, 5833.

[8] J. Yang, C.-R. Han, F. Xu, R.-C. Sun, *Nanoscale* **2014**, *6*, 5934.

[9] S. Lin, C. Cao, Q. Wang, M. Gonzalez, J. E. Dolbow, X. Zhao, *Soft Matter* **2014**, *10*, 7519.

[10] J. Yang, C.-R. Han, X.-M. Zhang, F. Xu, R.-C. Sun, *Macromolecules* **2014**, *47*, 4077.

[11] J. Li, Z. Suo, J. J. Vlassak, *J. Mater. Chem. B* **2014**, *2*, 6708.

[12] S. Lin, Y. Zhou, X. Zhao, *Extreme Mech. Lett.*, **2014**, *1*, 70.

[13] N. E. Fedorovich, J. Alblas, J. R. de Wijn, W. E. Hennink, A. J. Verbout, W. J. Dhert, *Tissue Eng.* **2007**, *13*, 1905.

[14] D. B. Kolesky, R. L. Truby, A. S. Gladman, T. A. Busbee, K. A. Homan, J. A. Lewis, *Adv. Mater.* **2014**, *26*, 3124.

[15] S. E. Bakarich, M. i. h. Panhuis, S. Beirne, G. G. Wallace, G. M. Spinks, *J. Mater. Chem. B* **2013**, *1*, 4939.

[16] J. S. Miller, K. R. Stevens, M. T. Yang, B. M. Baker, D.-H. T. Nguyen, D. M. Cohen, E. Toro, A. A. Chen, P. A. Galie, X. Yu, R. Chaturvedi, S. N. Bhatia, C. S. Chen, *Nat. Mater.* **2012**, *11*, 768.

[17] R. A. Barry, R. F. Shepherd, J. N. Hanson, R. G. Nuzzo, P. Wiltzius, J. A. Lewis, *Adv. Mater.* **2009**, *21*, 2407.

[18] B. Duan, L. A. Hockaday, K. H. Kang, J. T. Butcher, *J. Biomed. Mater. Res. Part A* **2013**, *101A*, 1255.

[19] L. A. Hockaday, K. H. Kang, N. W. Colangelo, P. Y. Cheung, B. Duan, E. Malone, J. Wu, L. N. Girardi, L. J. Bonassar, H. Lipson, C. C. Chu, J. T. Butcher, *Biofabrication* **2012**, *4*, 035005.

[20] R. S. Rivlin, A. G. Thomas, *J. Polym. Sci.* **1953**, *10*, 291.

[21] N. K. Simha, C. S. Carlson, J. L. Lewis, *J. Mater. Sci.: Mater. Med.* **2004**, *15*, 631.

[22] H. A. Bruck, S. R. McNeill, M. A. Sutton, W. H. Peters III, *Exp. Mech.* **1989**, *29*, 261.

[23] C. Y. Hui, A. Jagota, S. J. Bennison, J. D. Londono, *Proc. R. Soc. London A* **2003**, *459*, 1489.

[24] J. P. Gong, Y. Katsuyama, T. Kurokawa, Y. Osada, *Adv. Mater.* **2003**, *15*, 1155.

[25] C. Fan, L. Liao, C. Zhang, L. Liu, *J. Mater. Chem. B* **2013**, *1*, 4251.

[26] A. D. Rouillard, C. M. Berglund, J. Y. Lee, W. J. Polacheck, Y. Tsui, L. J. Bonassar, B. J. Kirby, *Tissue Eng., Part C* **2011**, *17*, 173.

[27] S. Khalil, J. Nam, W. Sun, *Rapid Prototyping J.* **2005**, *11*, 9.

[28] R. Chang, J. Nam, W. Sun, *Tissue Eng., Part A* **2008**, *14*, 41.

[29] C.-W. Chang, A. van Spreeuwel, C. Zhang, S. Varghese, *Soft Matter* **2010**, *6*, 5157.

[30] P. C. Thomas, B. H. Cipriano, S. R. Raghavan, *Soft Matter* **2011**, *7*, 8192.

[31] J. Wang, L. Lin, Q. Cheng, L. Jiang, *Angew. Chem. Int. Ed.* **2012**, *51*, 4676.

[32] S. Nemir, H. N. Hayenga, J. L. West, *Biotechnol. Bioeng.* **2010**, *105*, 636.

[33] W. H. Peters, W. F. Ranson, *OPTICE* **1982**, *21*, 213427.